

# A photometric and astrometric investigation of the brown dwarfs in Blanco 1

S. L. Casewell<sup>1\*</sup>, D .E. A. Baker<sup>1,2</sup>, R. F. Jameson<sup>1</sup>, S. T. Hodgkin<sup>3</sup>, P. D. Dobbie<sup>4</sup>, and E. Moraux<sup>5</sup>

<sup>1</sup>*Department of Physics and Astronomy, University of Leicester, University Road, Leicester LE1 7RH, UK*

<sup>2</sup>*Science & Technology Research Institute, University of Hertfordshire, College Lane, Hatfield AL10 9AB, UK*

<sup>3</sup>*CASU, Institute of Astronomy, University of Cambridge, Maddingley Road, Cambridge, CB3 0HA, UK*

<sup>4</sup>*University of Tasmania, Private Bag 50, Hobart, Tasmania 7001, Australia*

<sup>5</sup>*UJF-Grenoble 1 / CNRS-INSU, Institut de Planétologie et d'Astrophysique de Grenoble (IPAG) UMR 5274, Grenoble, F-38041, France*

16 October 2018

## ABSTRACT

We present the results of a photometric and astrometric study of the low mass stellar and substellar population of the young open cluster Blanco 1. We have exploited  $J$  band data, obtained recently with the Wide Field Camera (WFCAM) on the United Kingdom InfraRed Telescope (UKIRT), and 10 year old  $I$  and  $z$  band optical imaging from CFH12k and Canada France Hawaii Telescope (CFHT), to identify 44 candidate low mass stellar and substellar members, in an area of 2 sq. degrees, on the basis of their colours and proper motions. This sample includes five sources which are newly discovered. We also confirm the lowest mass candidate member of Blanco 1 unearthed so far ( $29M_{\text{Jup}}$ ). We determine the cluster mass function to have a slope of  $\alpha=+0.93$ , assuming it to have a power law form. This is high, but nearly consistent with previous studies of the cluster (to within the errors), and also that of its much better studied northern hemisphere analogue, the Pleiades.

**Key words:** stars: low-mass, brown dwarfs, open clusters and associations:individual:Blanco 1

## 1 INTRODUCTION

Open clusters are often acclaimed as excellent laboratories with which to study star formation. This is due to the co-eval nature of their members and estimates of their age being comparatively robust. Many open star clusters have been studied to date, yielding a large number of low mass members (e.g. Baker et al. 2010; Casewell et al. 2007; Lodieu et al. 2007) which have been used to refine our knowledge about the low mass end of star formation via mapping the initial mass function (IMF). The IMF, the number of objects per unit mass interval, is an observable outcome of star formation and can be used to critically examine theoretical models of this process. The IMF is commonly measured using an  $\alpha$  parameter, where  $dN/dM \propto M^{-\alpha}$  and  $N$  is number of objects, and  $M$  is mass. For most open star clusters (ages  $\sim 100$  Myr),  $\alpha$  is roughly consistent across all samples and  $\approx 0.6$  (Bouvier et al. 2005). This value is also consistent with field values such as those of Chabrier (2003), although recently it has been suggested that for very low mass field brown dwarfs the IMF may have a different form. In-

deed Burningham et al. (2010) suggest that in this case  $\alpha$  may even have a negative value.

In recent years there has been a particular emphasis on building a solid comprehension of the mechanisms by which very low mass brown dwarfs and free-floating planetary mass objects form (e.g. Bate 2011). Nevertheless, key questions remain to be answered e.g. what is the lowest possible mass of object that can be manufactured by the star formation process? From a theoretical stance, traditional models predict that if substellar objects form like stars, via the fragmentation and collapse of molecular clouds, then there is a strict lower mass limit to their manufacture of  $0.007\text{--}0.010 M_{\odot}$ . This is set by the rate at which the gas can radiate away the heat released by the compression (e.g. Low & Lynden-Bell 1976). However, in more elaborate theories, hypothetical magnetically mediated rebounds in collapsing cloud cores might lead to the decompressional cooling of the primordial gas, a lowering of the Jeans mass and hence the production of gravitationally bound fragments with masses of only  $\sim 0.001 M_{\odot}$  (Boss 2001).

However, while many surveys of open star clusters have been performed to search for substellar members, the majority of these are in the heavily populated Northern hemisphere clusters. The lack of southern coverage from surveys (e.g. Sloan Digital Sky Survey

\* E-mail: slc25@le.ac.uk

York et al. 2000; UKIRT Infrared Deep Sky Survey Warren et al. 2007) has impeded detailed studies of the substellar population of a plethora of potentially interesting southern open clusters.

Blanco 1 is a  $90 \pm 25$  Myr (Panagi & O’dell 1997) open cluster with an age similar to that of the 125 Myr Pleiades cluster (Stauffer, Schultz & Kirkpatrick 1998) at a distance of  $207 \pm 12$  pc as determined from *Hipparcos* measurements (van Leeuwen 2009). Recent work on the cluster includes spectroscopy of F and G type stars (Ford et al. 2005) which show that the metallicity is  $[Fe/H] = +0.04$ , with subsolar abundances for  $[Ni/Fe]$ ,  $[Si/Fe]$ ,  $[Mg/Fe]$ , and  $[Ca/Fe]$ . Cargile, James & Jeffries (2010) have determined a Lithium age for the cluster of  $132 \pm 24$  Myr which is closer to the age of the Pleiades than that of Panagi & O’dell (1997). We have taken the age of the cluster to be 120 Myr which is close to both measured values, and is present in the Chabrier et al. (2000) DUSTY models.

Recently Platais et al. (2011) surveyed 11 square degrees of the cluster to provide a comprehensive proper motion catalogue for all stellar objects down to M5V. Moraux et al. (2007) performed the first study of the cluster to search for brown dwarfs using CFH12k on the Canada-France-Hawaii Telescope in the optical  $z$  and  $I$  bands to image 2.3 square degrees of the cluster centre. They discovered  $\approx 300$  cluster members; 30-40 were estimated to be brown dwarfs, some of which had additional  $K$  band photometry and optical spectroscopy. Three of these objects were subsequently confirmed as members by Cargile et al. (2010).

We have used the  $I$  and  $z$  band images from Moraux et al. (2007) and have combined them with additional deep ( $J \approx 22$ )  $J$  band photometry obtained using WFCAM on UKIRT allowing us to not only select fainter candidate cluster members, but also to measure the proper motion for some of the previously identified objects to prove if they are indeed associated with the cluster.

## 2 OBSERVATIONS AND DATA REDUCTION

### 2.1 CFHT12K data

The initial Blanco 1 data was taken with the CFHT12k optical mosaic camera during two separate runs as detailed in Moraux et al. (2007). The first of the runs occurred between 30 September 1999 and 2 October 1999, with the second occurring between 18 and 20 of December 2000. A total of 7 fields were observed covering an area of 2.3 square degrees, in a (mostly) non overlapping pattern. Each separate field covered an area of  $28' \times 42'$ . The area of sky covered is shown in Figure 1. For each filter, Mould  $I$  and  $z$  Prime (see <http://www.cfht.hawaii.edu/Instruments/Filters/cfh12k.html> for filter profiles), a short observation of 10 s was accompanied by two longer 600 s exposures. These were then combined to produce an equivalent image containing 1200s worth of exposure. The detection limits of the data were  $I \sim z \sim 24$  (Moraux et al. 2007), well below the stellar/substellar boundary which for Blanco 1 is estimated to lie at  $I \approx 19.15$ . The reduction of the initial data by Moraux et al. (2007) followed the same prescription as described in Moraux et al. (2003).

The raw CFHT12k data frames were extracted from the Canadian Astrophysical Data Centre (CADC) archive and were reduced using the imaging pipeline (Irwin & Lewis 2001) following the procedures described in Casewell et al. (2007). Subsequently the two 600s images in each filter at each pointing were co-added prior to source extraction and catalogue generation. Sources

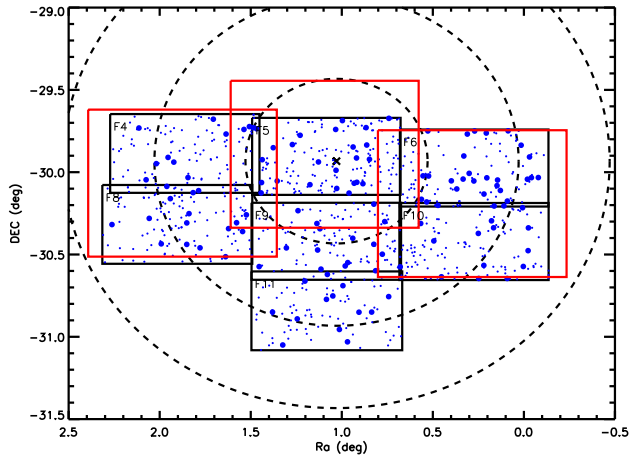


**Figure 1.** Outline of the sky coverage of Blanco 1 from the CFHT12k tiles (black) and the WFCAM tiles (red), the low-mass and very-low-mass candidate lists of Moraux et al. (2007) are shown as the small and large blue dots respectively. The black cross indicates the cluster centre, with circles of radius 0.5, 1.0 and 1.5 degrees being shown by the dashed black lines.

were identified as having a minimum of 5 interconnected pixels sitting at a significance of  $1.5\sigma$  above the background, with aperture photometry carried out using a radius of 3.5 pixels. In addition a morphological classification flag was provided with -1 indicating a stellar like profile, 0 noise and +1 non-stellar like sources. For the field-filter-extension/chip combinations of F4- $I$ -10, F4- $z$ -10, F6- $I$ -6, F6- $z$ -6 and F8- $I$ -8 the astrometry needed further correction to that supplied by the CASU pipeline which was accomplished by using “AAA” rated stars in 2MASS.

To refine the photometric calibration used by Moraux et al. (2003) which was based on A0 stars, we calculated a zero point for each chip in each filter using data from ESO.

Blanco 1 formed part of a study of young open clusters by the Monitor project (e.g. Irwin et al. 2008, 2009 and references therein). The observations were obtained using the MPG/ESO 2.2-m telescope with WFI in service mode, with around 500 epochs measured between July 2005 and October 2007 for four pointings (See Figure 2). The instrument provides a field of view of  $\sim 34 \times 33$  arcmin<sup>2</sup> ( $0.31$  deg<sup>2</sup>), using a mosaic of eight  $2k \times 4k$  pixel CCDs, at a scale of  $\sim 0.238$  arcsec pix<sup>-1</sup>. The filter used was the ESO WFI broadband  $I$  filter (designated BB# 1203\_ESO879, also known as the  $I_{EIS}$  filter) with a central wavelength of 826.9nm, and a sharp cutoff in the red shortwards of 950nm.

For a full description of the data reduction steps, the reader is referred to Irwin et al. (2007). Briefly, we used the pipeline for the INT wide-field survey (Irwin & Lewis 2001) for 2D instrumental signature removal (bias correction, flat-fielding, defringing) and astrometric and photometric calibration. We then generated a master catalogue for each filter by stacking 20 of the frames taken in the best conditions (seeing, sky brightness and transparency) and running the source detection software on the stacked image. Astrometric calibration is tied into 2MASS and has residuals of better than 0.05 arcseconds per pointing. Photometric calibration of our data was carried out using regular observations of Landolt (1992) equatorial standard star fields, measured as part of the standard ESO nightly calibrations. Prior to applying the calibration, we converted the Landolt (Cousins) photometry into the  $I_{EIS}$  system us-

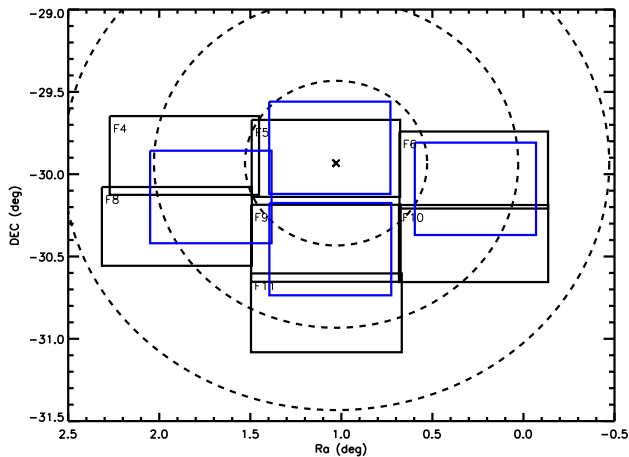


**Figure 2.** Outline of the coverage of Blanco 1 offered by the Monitor project data compared to the coverage given by the original CFHT12k fields.

ing colour equations from Mike Irwin (private communication), see Equation 1

$$I_{EIS} = I - 0.03(V - I) \quad (1)$$

(and also Irwin et al. 2008). By converting the Landolt standards into the *EIS* system, and working entirely in the natural system of the instrument, this stage of the calibration of the CCD photometry is independent of the differences in colour between the cluster members which are somewhat redder than the Landolt standards.

The *I* and *z* zeropoints used to calibrate the CFHT data were then calculated by comparing the uncalibrated instrumental magnitudes against those from the Monitor project. Data from each of the 12 CFHT12k CCDs were binned for each of the two separate runs, i.e. all the objects found on chip 6 (over the different fields) taken in the 1999 run were combined to provide one single photometric zero-point for that chip. As small regions of overlap exist between some of the CFHT12k fields, a test of photometric accuracy was conducted for those objects with duplicate detections. This yielded RMS values of  $\approx 0.035$  and  $\approx 0.040$  for the *z* and *I* filters respectively.

To confirm the calibration we first attempted to use the APASS survey (<http://www.aavso.org/apass>), however, there was insufficient overlap in magnitudes (the survey objects are saturated in the CFHT image) for us to use these data. We then cross-correlated the objects from Moraux et al. (2007) with our data and used them to check the calibration. We obtain an offset of  $I = +0.066 \pm 0.018$  and  $z = +0.080 \pm 0.012$  between the original CFHT data and our reprocessed images, with the original data being fainter. This is marginally larger than the RMS scatter, but is in general smaller than the errors on the measurements, and so we are satisfied that our calibration is accurate.

Following the photometric calibration, the separate *I* and *z* catalogues for each CFHT12k CCD chip were merged. This was done by using a flux limited sample of objects that had been morphologically classified as stellar. This subset was used as an input for pattern matching and linear transformation equation generation between the associated *x* and *y* pixel coordinates of the objects. Once a transformation had been established for the “clean” sample it was used to match the full sample together helping to reduce the number of spurious detections between the two images.

## 2.2 WFCAM data

In addition to the optical data, near-IR observation were also taken. Three WFCAM (Casali et al. 2007) *J* band tiles were obtained in UKIRT service mode, 2 on the night of 31 October 2006 and 1 on the night of 22 July 2009. Each WFCAM pawprint used exposures of 18 s and a 9 point jitter pattern with 2x2 microstepping to improve the spatial sampling, making 1 hour of observations in total per tile: 600s exposure per pawprint, in seeing of  $\approx 1''$  or better. The WFCAM data was processed as for the Pleiades survey of Casewell et al. (2007). The calibration and pipeline for the data reduction are described in Hodgkin et al. (2009). The photometric calibration is tied to 2MASS photometry resulting in accuracies of  $\sim 1.5$  per cent. The total area covered by the WFCAM fields is 2.25 square degrees, of which  $\approx 2$  square degrees overlaps with the CFHT12k data as shown in Figure 1.

The CFHT12k data was pattern matched to the WFCAM data on an individual field by field, chip by chip basis to minimise multiple detections. Each source also had to be classified as stellar in both the CFHT12k *I* and *z* band images as well as the WFCAM *J* band image. The resulting catalogue contained 9853 sources (8440 of which were unique).

We estimated the completeness of both the CFHT12k and WFCAM images using the method described in Casewell et al. (2007). We inserted 200 fake stars ( $12 < J < 22$ ,  $15 < I, z < 30$ ) generated by IRAF into each chip, 10 times to enable us to have sufficient objects on which to perform the statistics. The sky level, detector gain, seeing, exposure times and zeropoint of the images was taken into account when creating the fake stars. The CASU routine IMCORE was used to extract the objects from each image and then the numbers of inserted and extracted objects were compared per magnitude bin. The data were found on average to be 90 per cent complete at 19.73 in the *J* band, and 21.5 and 20.6 in the *I* and *z* bands respectively, and 50 per cent complete at 20.8 in *J* and 22.2 and 21.5 in the *I* and *z* bands respectively. In general it was found that chip number 4 of WFCAM was about 0.2 mags less sensitive than the other 3 chips.

## 3 RESULTS

### 3.1 Photometric selection

For consistency with previous studies of objects within this effective temperature range we chose to use the DUSTY models of Chabrier et al. (2000). We selected all sources with *I-J* within 0.5 of each side of the model for 120 Myrs at 207 pc. This selection allows for uncertainty in distance and the equal mass binary sequence. We then applied additional selection criteria of  $I - J > 1.95$  and  $z - J > 1.15$  to extract the sequence from the bulk of the field stars. Figure 3. We selected a total of 83 objects using this method.

To determine the accuracy of our selection criteria, we compared how many of the objects presented in Moraux et al. (2007) were recovered by our survey. Moraux et al. (2007) present 764 unique sources, titled Low Mass Candidates (LMC) and Very Low Mass Candidates (VLMC), 578 of which are located within our survey area. Many of these objects were discovered using short exposures of 10s and so are saturated in our data (1200 s in the *I* and *z* bands). To allow for this, and to better exploit our deeper data, we then applied a bright limit of  $I = 18.5$  in our selection criteria. We recovered 522 objects in our survey area before the selection criteria were applied. The missing  $\approx 50$  objects have not been recovered due to falling between chip gaps, or not being detected in

our  $J$  band data as they are not red enough to be cluster members. Of the very low mass candidates, 81 are covered by our survey, and we recover all of these objects in our data.

However, after the selection cuts were made, only 27 LMC objects remained and 38 VLMC objects although there is some overlap between the lists (Table A1; Appendix A). The remainder were lost as they were brighter than  $I = 18.5$ , or fell outside the strip defined by the model i.e. despite appearing to belong to the cluster sequence in  $I - z$ , they do not appear to belong to the sequence in  $I - J$  or  $z - J$  (generally being too blue), and so are probably not members of the cluster.

### 3.2 Proper motions and membership probabilities

We measured the proper motions of the 83 selected objects using the  $z$  and  $J$  bands, which gave an epoch difference of 10 years for the majority of objects, although a handful had a shorter epoch difference of only 8 years. The  $z$  band was chosen over the  $I$  band to minimise any effects of differential chromatic refraction as all images were taken at high airmass, due to Blanco 1 being near the observing limits of both UKIRT and CFHT. We used a pixel-pixel transformation routine that uses a set of stationary reference sources in each image as described by Casewell et al. (2007). The reference objects were selected to have magnitudes  $16 \leq \text{mag} < 20$  in  $z$ , similar to that of the candidates, but not so faint as to have poor pixel centroiding. It was also required that they have an ellipticity of less than 0.2 in the  $z$  band image and be located within  $10'$  of the candidate to minimise radial distortion effects. In regions of overlap it was also ensured that the candidate be on the same chip as the reference stars in each image.

Centroiding errors were estimated using fake stars as for the completeness calculations, only this time the difference in pixel positions between the inserted and recovered stars was measured. This difference was measured in magnitude bins, as it was anticipated that fainter objects would have larger centroiding errors. These errors were 0.01 pixels in  $J$  for  $J < 17.0$  and 0.07 for  $J > 17.0$ , where the detector pixel size is  $0.4''$ . For the  $z$  band, the errors were 0.03 for  $z < 23.0$ , where the detector pixel size is  $0.2''$ . These pixel measurements were added quadratically to the rms error on the pixel-pixel transforms to generate the proper motion errors.

Centroiding errors were estimated using fake stars as for the completeness calculations, only this time the difference in pixel positions between the inserted and recovered stars was measured. This difference was measured in magnitude bins, as it was anticipated that fainter objects would have larger centroiding errors. These errors were 0.01 pixels in  $J$  for  $J < 17.0$  and 0.07 for  $J > 17.0$ , where the detector pixel size is  $0.4''$ . For the  $z$  band, the errors were 0.03 for  $z < 23.0$ , where the detector pixel size is  $0.2''$ . These pixel measurements were added quadratically to the rms error on the pixel-pixel transforms to generate the proper motion errors.

Once we had measured the proper motions, the data were then binned in  $10 \text{ mas yr}^{-1}$  bins in both RA and dec, and a 2D Gaussian was fitted to the data in proper motion space. The  $\sigma$  derived was then used to reject objects outside the  $2\sigma$  boundary to remove outliers, and the fit was then recalculated. This gave a Gaussian width of  $\sigma \sim 9.0 \text{ mas yr}^{-1}$  to be used for candidate selection.

It is obvious from Figure 4 that the average proper motion of our selected objects ( $\mu_{\alpha \cos \delta} = 8.93 \text{ mas yr}^{-1}$ ,  $\mu_{\delta} = 6.70 \text{ mas yr}^{-1}$ ) is significantly different from the literature value of the cluster proper motion ( $\mu_{\alpha \cos \delta} = 20.11 \text{ mas yr}^{-1}$ ,  $\mu_{\delta} = 2.43 \text{ mas yr}^{-1}$ ; van Leeuwen 2009). Platais et al. (2011) determined that the mean motion of field stars is not at 0,0 as is generally used for relative proper motions, but at  $\mu_{\alpha \cos \delta} = 8.0 \text{ mas yr}^{-1}$ ,  $\mu_{\delta} = -6.0 \text{ mas yr}^{-1}$ . To determine if this offset was applicable to our data we modified our photometric selection criteria to obtain everything 0.5 mag bluer in  $I - J$  than the Dusty model (Chabrier et al. 2000). We then measured proper motions for these 250 objects, and fitted a 2D Gaussian to their proper motions as before. We determined that the centre of this distribution is at  $\mu_{\alpha \cos \delta} = 1.96 \text{ mas yr}^{-1}$ ,  $\mu_{\delta} = -3.64 \text{ mas yr}^{-1}$ , with a width of  $12 \text{ mas yr}^{-1}$ . This motion is smaller than that measured by Platais et al. (2011), but they measured many more stars, and to a better accuracy than this work which has con-

centrated on the fainter members of the cluster. This mean motion explains the offset between our candidate distribution and the cluster motion. Taking into account the offset makes our mean proper motion  $\mu_{\alpha \cos \delta} = 16.93 \text{ mas yr}^{-1}$ ,  $\mu_{\delta} = 0.70 \text{ mas yr}^{-1}$  which is much closer to the reported value for the cluster. We used the literature value of the cluster proper motion, minus the Platais et al. (2011) estimation of the field star motion,  $\mu_{\alpha \cos \delta} = 12.11 \text{ mas yr}^{-1}$ ,  $\mu_{\delta} = 8.43 \text{ mas yr}^{-1}$ , as the cluster centre for selection purposes. It should also be noted that the field and cluster stars are not that far apart in terms of the relative errors which Platais et al. (2011) discuss in more depth in their work on Blanco 1. Despite the small difference between the proper motion of the cluster and field stars, the narrower dispersion in proper motion for the cluster objects, and the colour selections in  $I - J$  and  $z - J$  mean we can be confident that we are selecting true cluster members.

Of the 83 candidates for which we obtained astrometry, 44 had proper motions within (or with errors within)  $3\sigma$  of the cluster value adjusted to take into account the field star relative motion ( $\mu_{\alpha \cos \delta} = 12.11 \pm 0.38$ ,  $\mu_{\delta} = 8.43 \pm 0.25$ ; Platais et al. 2011; van Leeuwen 2009). Of these 44 members, 33 are present in the VLMC list and 24 are present on the LMC list, with 18 objects common to both lists of candidate sets. This leaves 5 new low-mass candidate members to the cluster. The previously identified objects that were rejected are LMC694/VLMC66, VLMC64, VLMC68, VLMC69, VLMC71 and VLMC74. All VLMC objects with spectra remain in our candidates apart from objects 29,38,48 and 49 which are not in our survey area, and 16 and 22 which did not meet our photometric selection criteria (they are too bright). It should be noted that the 3 objects identified by (Moraux et al. 2007) as non-members based upon their spectroscopy, VLMC28, 37 and 44 were not selected, (VLMC28 also does not have a spectrum indicative of it being a cluster member; Cargile et al. 2010). The success of this method in recovering the previously identified spectroscopic members, despite large errors on the small cluster proper motion, leads us to believe this is a robust method for determining cluster members.

Examining the proper motion vector point diagram (Figure 4) it is clear that towards the location of the cluster there is an over-density of objects when compared with regions at a similar distance from 0,0 but on the opposing side of the field star distribution. Unfortunately, the low number of sources coupled with a cluster proper motion comparable to the average proper motion error means that the two Gaussian approach to calculating membership probability as used by Baker et al. (2010) is not applicable. Instead the simpler annulus method was used as in Casewell et al. (2007). All non-selected objects with measured proper motions (barring those where there has obviously been a problem with the fit - 7 cases) were used per  $I$  magnitude bin to assess the contamination and membership probabilities. We were unable to use an annulus centred on 0,0 as there are very few objects there not deemed to be members of Blanco 1 due to the low proper motion of the cluster. This may mean that some of the membership probabilities have been underestimated (Table 1).

## 4 MASS SPECTRUM

We were not able to generate mass functions for our new candidate members alone, due to there being too few objects to be statistically significant. However, we have used the Moraux et al. (2007) members combined with the  $I - z$  colour and the NextGen model (Baraffe et al. 1998) for objects brighter than  $I=20.0$ , and

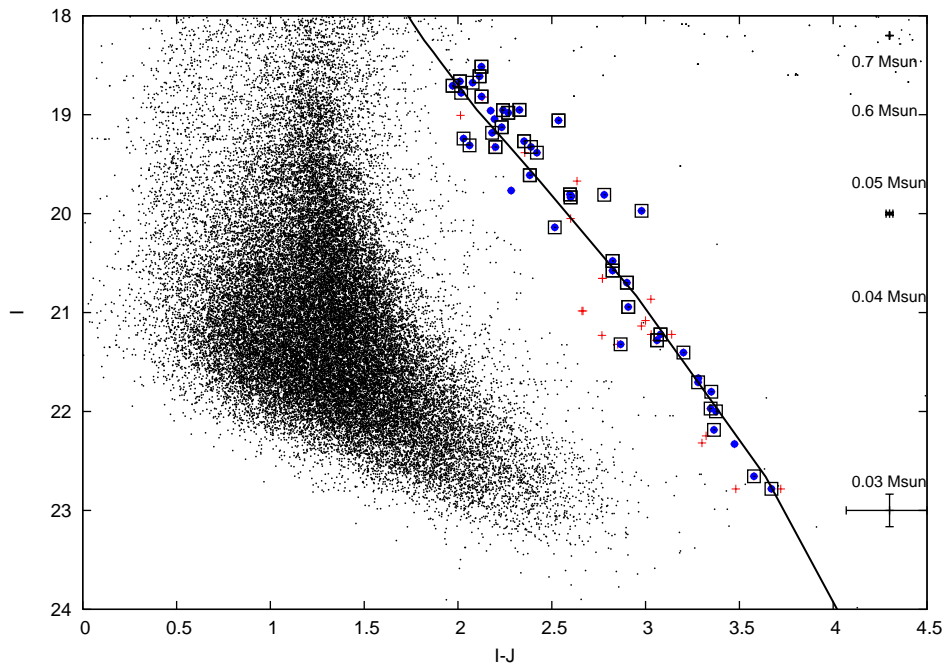


**Figure 3.** Colour magnitude selections in  $I$ ,  $I - J$ . The black points are the stellar CFHT12k-WFCAM sources. Red + mark the selected objects, while large blue filled circles indicate objects that remained after the proper motion selection. The objects identified as candidate members from Moraux et al. (2007) are marked by boxes. Representative errorbars and masses are also shown, as is the DUSTY model isochrone for 120 Myr Chabrier et al. (2000).

**Table 1.** Magnitude bins and the associated membership probability and completeness at this  $I$  magnitude.

$I$	Probability	Completeness
<19.5	91%	100%
19.5-20.5	75%	97%
20.5 to 21.5	50%	93%
21.5-22.5	50%	62%
>22.5	40%	16%

the DUSTY model (Chabrier et al. 2000) for object fainter than this. Both models are for 120 Myr. We present 3 mass spectra, one the original data from Moraux et al. (2007), and the second with the non-members, as determined from this work, excluded. The third dataset is all the members, including our 5 new objects (Figure 5). These new objects have masses between  $35 M_{\text{Jup}}$  and  $46 M_{\text{Jup}}$ , whereas the whole mass range of candidates is between 29 and  $80 M_{\text{Jup}}$ . The third dataset (filled circles) is fitted by the straight line in Figure 5, with an  $\alpha$  value of  $0.93 \pm 0.11$ . However, to obtain this fit, we have omitted the point at  $\log M = -1.85$ : the faintest objects and lowest mass bin where we know the incompleteness is largest. We do not have a good enough photometry to accurately separate the single and binary star sequences, and thus suspected binaries have been assigned a mass equivalent to that of a single object at their recorded magnitude. The point at  $\log M = -0.85$  is discrepantly high and appears to be affected by binaries and possibly higher multiples at  $I \approx 20$  (Figure 3).

The  $\alpha = 0.93 \pm 0.11$  indicates the slope is higher, but is consistent (to within the errors) with the values given by Moraux et al. (2007), which are  $0.67 \pm 0.14$  and  $0.71 \pm 0.13$  for 100 and 150 Myr models respectively, especially considering we have small number statistics in some mass bins.

While we have discovered 5 new low mass cluster members, our  $J$  band data did not allow us to probe deeper into Blanco 1 than the original  $Iz$  survey by Moraux et al. (2007). This situation will be improved as the VISTA VIKING survey which aims to cover the whole of the Blanco 1 cluster. It will also provide deeper multi-band photometry, as well as a far greater baseline between observations to be used for proper motion analysis. Our work has shown that Blanco 1 does contain brown dwarfs as low in mass as  $\sim 30 M_{\text{Jup}}$ , making it similar to the Pleiades.

Follow up spectroscopic data will allow us to place constraints on the binary fraction of the cluster, as well as confirm membership for the objects without spectra. Decreasing the errors on the proper motions will allow us to determine members with much more confidence than we are currently able to due to the low space motion of the cluster. Once a full census of the cluster has been performed, Blanco 1 can then be properly compared to clusters such as the Pleiades. One can then test for the environmental tolerance of the IMF, dynamical evolution and mass segregation effects as well as providing further observational constraints to compare with the results of brown dwarf formation simulations.

## 5 SUMMARY

We have used near-IR and optical photometry with proper motions derived from CFHT  $z$  and WFCAM  $J$  band images to identify 44 candidate cluster members with masses between  $29 M_{\text{Jup}}$  and  $80 M_{\text{Jup}}$ . 5 of these are previously unidentified candidate members and 40 have been identified by Moraux et al. 2007, 8 of which have been confirmed as cluster brown dwarfs from spectra. We derive  $\alpha = 0.93 \pm 0.11$  from the mass spectrum, which is consistent with the literature for this cluster.

**Table 2.** Name, Moraux et al. (2007) name, coordinates, proper motion,  $I$ ,  $z$ ,  $J$  magnitudes for our members to the cluster. Previously discovered members also also have their other known names listed. An asterisk (\*) indicates that membership has been confirmed from Moraux et al. (2007) spectroscopy.

Name	Alternate name	RA J2000.0	dec	$\mu_{\alpha} \cos \delta$ mas yr $^{-1}$	$\mu_{\delta}$	$I$	$z$	$J$
bl2399-4716		00 00 6.83	-30 13 33.72	+2.27 ±12.96	+20.66 ±11.56	19.045±0.010	18.201±0.033	16.851±0.007
bl28626-47167	LMC571/VLMC19	00 07 50.63	-30 5 9.97	+7.45 ±6.86	+5.90 ±5.45	18.515±0.013	17.688±0.037	16.391±0.005
bl2868-4699	VLMC89	00 00 5.86	-30 20 18.39	+13.99 ±8.10	+14.07 ±7.33	21.971±0.050	20.755±0.073	18.625±0.027
bl28691-43204	VLMC54	00 07 41.46	-29 56 20.39	+31.93 ±5.57	-7.13 ±3.81	19.971±0.017	18.782±0.041	16.993±0.008
bl32426-33057	LMC629/VLMC46	00 05 57.04	-29 43 48.33	-1.93 ±4.90	-26.66 ±13.69	19.328±0.015	18.431±0.039	17.128±0.009
bl32697-33301	LMC729/VLMC72	00 06 8.96	-29 44 25.22	+2.45 ±22.41	+16.06 ±6.60	21.280±0.029	20.035±0.054	18.219±0.019
bl33600-62347	LMC626	00 06 41.73	-29 42 52.52	-13.07 ±13.81	-7.03 ±9.07	19.310±0.015	18.466±0.039	17.248±0.009
bl33721-62566	LMC705/VLMC63	00 06 49.36	-29 40 41.18	+10.90 ±8.92	+12.40 ±10.72	20.698±0.022	19.521±0.046	17.798±0.013
bl34536-62053	VLMC118	00 06 32.59	-29 46 05.57	+11.29 ±9.71	+12.87 ±8.17	22.782±0.086	21.357±0.097	19.111±0.037
bl37640-49624	LMC592/VLMC30	00 08 27.38	-29 43 54.26	+10.94 ±18.20	+17.94 ±18.40	18.708±0.014	17.965±0.037	16.737±0.006
bl3800-15178	LMC580/VLMC25*	00 00 42.74	-30 17 43.43	+6.40 ±13.62	+10.82 ±6.75	18.612±0.010	17.779±0.032	16.497±0.006
bl3819-15319	LMC621	00 00 36.44	-30 19 15.95	+22.62 ±13.28	+6.14 ±5.19	19.184±0.011	18.288±0.033	17.002±0.008
bl43328-55651	VLMC57	00 07 22.76	-30 01 57.32	-4.16 ±14.08	+1.65 ±8.34	20.139±0.018	18.952±0.043	17.623±0.012
bl44742-27543	VLMC82	00 04 42.00	-30 04 33.52	+11.93 ±4.88	-3.91 ±1.70	21.704±0.041	20.497±0.058	18.425±0.034
bl46456-37665	VLMC70	00 05 45.83	-30 03 46.14	+24.71 ±12.74	+7.79 ±11.09	21.221±0.028	20.031±0.049	18.142±0.019
bl51473-23799	LMC582/VLMC26	00 04 54.98	-29 46 32.88	+7.79 ±10.99	+11.10 ±16.02	18.663±0.010	17.935±0.031	16.653±0.006
bl51714-24041	LMC719/VLMC67	00 05 05.19	-29 49 55.81	+13.41 ±14.08	+17.17 ±6.20	20.943±0.025	19.925±0.042	18.035±0.016
bl54505-36470		00 03 24.26	-30 00 51.66	+0.82 ±16.17	+18.36 ±17.75	18.959±0.010	18.094±0.031	16.785±0.007
bl54514-36502	LMC608/VLMC41*	00 03 23.62	-29 55 17.56	+0.00 ±0.63	-0.00 ±0.63	19.058±0.010	18.033±0.031	16.522±0.006
bl54613-36058	LMC663/VLMC60	00 03 40.17	-30 03 40.85	-0.57 ±11.55	-10.33 ±4.90	20.478±0.017	19.384±0.038	17.654±0.012
bl54805-35986	VLMC74	00 03 43.78	-30 04 01.66	+26.29 ±3.66	+32.89 ±3.99	21.404±0.030	20.167±0.047	18.202±0.019
bl55543-35398	LMC645/VLMC51*	00 04 07.62	-29 59 18.78	+3.57 ±6.12	+3.91 ±9.53	19.806±0.014	18.782±0.036	17.210±0.009
bl56159-35803		00 03 50.87	-30 01 58.01	+17.68 ±3.98	+12.55 ±5.98	22.329±0.070	21.084±0.087	18.855±0.032
bl56339-2865	LMC624/VLMC45*	00 01 35.71	-30 03 10.13	+18.36 ±6.54	+1.41 ±6.49	19.268±0.012	18.326±0.033	16.915±0.008
bl57823-3435	VLMC114	00 02 5.68	-30 01 23.65	+10.59 ±8.078	+8.75 ±5.89	22.655±0.110	21.382±0.105	19.077±0.042
bl57973-12146	LMC647/VLMC55	00 02 15.12	-30 09 52.64	-1.94 ±2.57	+10.56 ±11.70	19.835±0.016	18.843±0.036	17.235±0.009
bl58756-8496	VLMC65	00 00 7.31	-29 54 26.81	-2.81 ±9.46	+15.26 ±14.08	20.575±0.021	19.495±0.043	17.751±0.015
bl6053-16818	VLMC53	00 02 16.10	-30 18 41.03	+13.82 ±14.46	+8.77 ±9.38	19.810±0.013	18.747±0.034	17.031±0.008
bl60868-7134	VLMC32	00 01 19.28	-29 54 06.58	+57.44 ±25.62	-4.17 ±14.72	18.779±0.010	17.991±0.031	16.762±0.007
bl63549-4173	LMC639/VLMC50*	00 00 9.86	-30 01 59.39	-9.78 ±19.95	+1.10 ±12.38	19.612±0.013	18.651±0.034	17.229±0.011
bl65492-14209	VLMC83	00 00 34.79	-30 02 51.04	+21.52 ±0.63	+14.18 ±0.63	21.800±0.044	20.494±0.059	18.450±0.026
bl71077-57153	LMC609/VLMC36*	00 07 08.79	-30 06 42.35	+7.29 ±6.58	+2.57 ±6.10	18.958±0.014	18.072±0.038	16.713±0.006
bl73194-41854	LMC632	00 08 13.55	-30 16 50.17	-12.48 ±11.52	-10.16 ±7.71	19.384±0.015	18.208±0.038	16.964±0.008
bl7507-10415	LMC585	00 00 12.10	-30 35 56.07	+6.15 ±8.99	+13.13 ±13.04	18.676±0.010	17.833±0.031	16.599±0.006
bl76145-40818	LMC595/VLMC33	00 06 10.79	-30 21 37.02	+3.23 ±11.65	+5.40 ±8.18	18.817±0.014	17.961±0.037	16.691±0.007
bl76187-40858		00 06 08.53	-30 25 42.12	-2.96 ±13.80	-9.37 ±13.61	19.767±0.017	18.851±0.040	17.483±0.011
bl76366-40509	VLMC75	00 06 29.32	-30 20 33.54	+4.38 ±14.23	-3.55 ±9.32	21.321±0.035	20.260±0.054	18.454±0.023
bl78357-42493	LMC631	00 07 33.84	-30 24 35.13	+9.32 ±9.17	+7.78 ±6.73	19.327±0.015	18.376±0.039	16.937±0.008
bl84053-20433		00 03 17.87	-30 11 40.93	+6.94 ±5.57	+18.65 ±3.55	21.663±0.037	20.350±0.052	18.382±0.023
bl85709-22911	LMC604/VLMC43*	00 04 32.88	-30 18 41.90	+9.41 ±11.43	+14.39 ±11.46	19.127±0.010	18.238±0.031	16.894±0.008
bl862-2266	LMC600/VLMC34*	00 01 48.76	-30 38 06.81	-3.19 ±7.45	-2.53 ±5.11	18.951±0.011	17.960±0.032	16.624±0.007
bl87593-22425	VLMC93	00 04 57.74	-30 14 02.01	+46.11 ±18.36	-0.75 ±18.34	22.186±0.073	20.903±0.058	18.822±0.034
bl89514-11054	LMC619	00 02 50.60	-30 28 53.89	-11.83 ±17.94	+9.38 ±11.27	19.241±0.011	18.429±0.033	17.211±0.010
bl90054-11175	VLMC85	00 03 06.63	-30 29 53.90	+4.08 ±6.31	+14.00 ±5.78	21.999±0.049	20.763±0.067	18.624±0.029

## 6 ACKNOWLEDGEMENTS

DEAB acknowledges support from STFC and SLC is supported by a University of Leicester post-doctoral research position. This paper made use of data from the United Kingdom Infrared Telescope which is operated by the Joint Astronomy Centre on behalf of the Science and Technology Facilities Council of the U.K. We would also like thank France Allard for the use of the Phoenix web simulator at <http://phoenix.ens-lyon.fr/simulator/index.faces> which has been used in this research. This research has also made use of NASA's Astrophysics Data System Bibliographic Services.

## REFERENCES

- Baker D. E. A., Jameson R. F., Casewell S. L., Deacon N., Lodieu N., Hambly N., 2010, *MNRAS*, 408, 2457
- Baraffe I., Chabrier G., Allard F., Hauschildt P. H., 1998, *A&A*, 337, 403
- Bate M. R., 2011, *MNRAS*, 417, 2036
- Boss A. P., 2001, *ApJL*, 551, L167
- Bouvier J., Moraux E., Stauffer J., 2005, in E. Corbelli, F. Palla, & H. Zinnecker ed., *The Initial Mass Function 50 Years Later* Vol. 327 of *Astrophysics and Space Science Library*, The 0.03-10  $M_{\odot}$  mass function of young open clusters. p. 61
- Burningham B., et al., 2010, *MNRAS*, 406, 1885

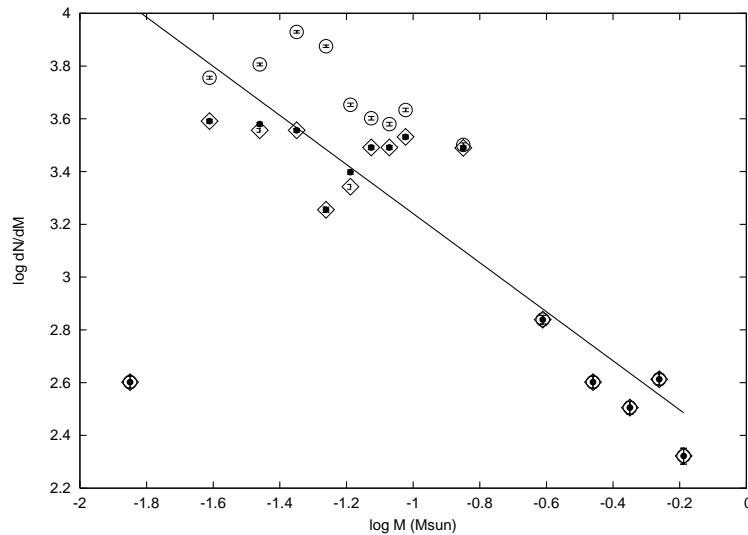


**Figure 5.** The mass spectrum for Blanco 1. The circles are the original members detailed by Moraux et al. (2007). It should be noted that the errors are poissonian, and in the case of the lowest mass bins, actually fall within the plotted point. The diamonds are the Moraux et al. (2007) objects, with non-members as determined from this work, removed. The filled circles are a complete mass function for all objects we determined to be members. The fit to the data of  $\alpha=0.93\pm 0.11$  is the solid line.

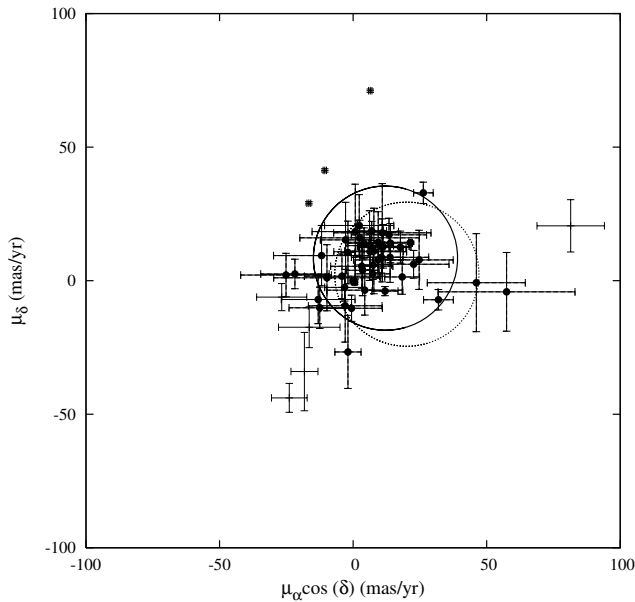


**Figure 4.** Proper motion diagram for the Blanco 1 cluster. Objects marked by a + are all objects we measured proper motions for. Objects marked by a filled circle are selected objects; they fall within a  $27 \text{ mas yr}^{-1}$  circle centred on the cluster proper motion once it has been adjusted for the field star motions ( $\mu_{\alpha \cos \delta} = 12.11 \text{ mas yr}^{-1}$ ,  $\mu_{\delta} = 8.43 \text{ mas yr}^{-1}$ ). The centre of the dotted circle shows the unshifted cluster proper motion ( $\mu_{\alpha \cos \delta} = 20.11 \text{ mas yr}^{-1}$ ,  $\mu_{\delta} = 2.43 \text{ mas yr}^{-1}$ ).

- Chabrier G., Baraffe I., Allard F., Hauschildt P., 2000, *ApJ*, 542, 464  
 Ford A., Jeffries R. D., Smalley B., 2005, *MNRAS*, 364, 272  
 Hodgkin S. T., Irwin M. J., Hewett P. C., Warren S. J., 2009, *MNRAS*, 394, 675  
 Irwin J., Aigrain S., Bouvier J., Hebb L., Hodgkin S., Irwin M., Moraux E., 2009, *MNRAS*, 392, 1456  
 Irwin J., Hodgkin S., Aigrain S., Bouvier J., Hebb L., Irwin M., Moraux E., 2008, *MNRAS*, 384, 675  
 Irwin J., Irwin M., Aigrain S., Hodgkin S., Hebb L., Moraux E., 2007, *MNRAS*, 375, 1449  
 Irwin M., Lewis J., 2001, *NewAR*, 45, 105  
 Landolt A. U., 1992, *AJ*, 104, 340  
 Lodieu N., Hambly N. C., Jameson R. F., Hodgkin S. T., Carraro G., Kendall T. R., 2007, *MNRAS*, 374, 372  
 Low C., Lynden-Bell D., 1976, *MNRAS*, 176, 367  
 Moraux E., Bouvier J., Stauffer J. R., Barrado y Navascués D., Cuillandre J., 2007, *A&A*, 471, 499  
 Moraux E., Bouvier J., Stauffer J. R., Cuillandre J., 2003, *A&A*, 400, 891  
 Panagi P. M., O'dell M. A., 1997, *A&AS*, 121, 213  
 Platais I., et al., 2011, *MNRAS*, 413, 1024  
 Stauffer J. R., Schultz G., Kirkpatrick J. D., 1998, *ApJL*, 499, L199+  
 van Leeuwen F., 2009, *A&A*, 497, 209  
 Warren S. J., et al., 2007, *MNRAS*, 375, 213  
 York D. G., et al., 2000, *AJ*, 120, 1579

- Cargile P. A., James D. J., Jeffries R. D., 2010, *ApJL*, 725, L111  
 Casali M., et al., 2007, *A&A*, 467, 777  
 Casewell S. L., Dobbie P. D., Hodgkin S. T., Moraux E., Jameson R. F., Hambly N. C., Irwin J., Lodieu N., 2007, *MNRAS*, 378, 1131  
 Chabrier G., 2003, *PASP*, 115, 763

**Table A1.** LMC and VLMC candidate members in our data, but determined to be non-members of the cluster due to photometry that was incompatible with our selection criteria.

Name	Name
LMC573	LMC678
LMC574	LMC679
LMC576	LMC682
LMC578	LMC683
LMC581/VLMC28	LMC684
LMC586	LMC685
LMC587	LMC686
LMC588	LMC688
LMC590	LMC689
LMC593	LMC690
LMC594	LMC692
LMC596	LMC695
LMC597	LMC699
LMC598	LMC700
LMC603/VLMC39	LMC702
LMC610	LMC704
LMC611	LMC707
LMC614	LMC708
LMC616	LMC709
LMC620	LMC710
LMC625	LMC711
LMC627	LMC712
LMC630	LMC713
LMC635	LMC715
LMC637	LMC716
LMC638	LMC717
LMC640	LMC718
LMC642	LMC720
LMC643	LMC721
LMC644	LMC722
LMC646	LMC724
LMC652	LMC725
LMC655/VLMC58	LMC726
LMC656	LMC727
LMC657	LMC728
LMC658	LMC730
LMC659	LMC732
LMC660	LMC735
LMC661	LMC736
LMC662	LMC738
LMC666	LMC739
LMC668	LMC741
LMC669	LMC747
LMC671	LMC749
LMC673	LMC752
LMC674	LMC755
LMC675	LMC762
LMC677	

**APPENDIX A: SUPPLEMENTARY TABLE**

Table A1 displays a list of the Low Mass Candidates (LMC) and Very Low Mass Candidates (VLMC) identified by Moraux et al. (2007), that were present in our survey area, but were rejected by our photometric selection.